millimeter wavelength circular waveguide system. It has been shown that the performance achieved with the presently installed waveguide exceeds the requirements of the original specification with regard to loss per unit length as a function of frequency, attenuation stability as a function of time and uniformity of the amplitude and phase frequency responses. Recently completed measurements on a further 15 km of waveguide installed on the north and southeast arms of the array show similar performance to that reported here.

In the present case, the direct burial technique has proven to be a most cost-effective means of installing a high performance low-loss waveguide transmission medium. Although the San Augustin basin is relatively geologically stable, the soil conditions over the extent of the array vary markedly from wet clay, with a high water table, to dry sandy earth. Therefore, it is felt that the method used for waveguide burial has played a major role in the achievement of stable, low-loss performance.

References

[1] S. Weinreb, R. Predmore, M. Ogai, and A. Parrish, "Waveguide system for a very large antenna array," *Microwave J.*, vol. 20, no. 3, pp. 49–52, Mar. 1977.
[2] J. W. Archer, M. Ogai, and E. M. Caloccia, "The sector coupler-theory and performance," submitted to IEEE-MTT in 1980.
[3] J. W. Archer, "Spurious responses in the VLA circular waveguide system," NRAO-VLA Electronics Memo 177, Aug. 1978.
[4] H. E. Rowe, and W. D. Warters, "Transmission in multimode waveguide with random imperfections," *Bell Syst. Tech. J.*, vol. 41, pp. 1031–1170, May 1962.
[5] J. W. Archer, "TE_{0n} mode filters for the VLA circular waveguide system," *Electronics Lett.*, vol. 15, no. 12, p. 343, June 1979.
[6] D. S. Heeschen, "The very large array," *Sky and Telescope*, vol. 49, pp. 334–351, Mar. 1975.

A Swept-Frequency Magnitude Method for the Dielectric Characterization of Chemical and Biological Systems

MARK A. HOLLIS, STUDENT MEMBER, IEEE, CARL F. BLACKMAN, CLAUDE M. WEIL, MEMBER, IEEE, JOHN W. ALLIS, AND DANIEL J. SCHAEFER, STUDENT MEMBER, IEEE

***Abstract*—A swept-frequency system is described which permits the convenient evaluation of many RF parameters of biological and chemical samples. This system is capable of highly accurate magnitude measurements which can provide not only absorption information but also the complex permittivity when processed through a computerized algorithm. Data have been taken on deionized water and on an aqueous triglycine solution, and there is close agreement with the more time-consuming but precise fixed-frequency measurements of cited references. This measurement system is particularly useful for the examination of frequency- and power-specific responses over narrow ranges.**

I. Introduction

RESEARCH into the biological effects of electromagnetic radiation has been hampered by the lack of a satisfactory ability to find probable frequencies and field intensities of interaction between nonionizing radiation and biological systems. Many experiments have been conducted using exposure frequencies and field strengths selected for convenience or availability of equipment. Recent evidence suggests that there are not only modulation dependencies [1],[2] but power-effect windows [1]–[3] for the EM field-stimulated responses of several biological tissues. These results point out the importance of having prior knowledge of effective modulation parameters, carrier frequencies, and field intensities when experiments are designed. The measurement of the relatively broad Debye relaxation spectra of biological molecules in aqueous solution can provide at least part of this information, but some workers [4], [5] suggest that there may be very narrow-band power-specific small-magnitude changes in the electrical properties of several biochemical systems. A satisfactory measurement system must have enough sensitivity and frequency resolution to detect these small changes, yet it must possess a broad-band capability which will enable convenient studies of Debye spectra.

At least two measurement methods have been published which meet these basic criteria. An automated network analyzer approach developed by Swicord [5] shows prom-

Manuscript received August 23, 1979; revised January 24, 1980.

M. A. Hollis was with the Health Effects Research Laboratory, U.S. Environmental Protection Agency, Research Triangle Park, NC. He is now with the School of Electrical Engineering, Cornell University, Ithaca, NY 14853.

C. F. Blackman, C. W. Weil, J. W. Allis, and D. J. Schaefer are with the Health Effects Research Laboratory, U.S. Environmental Protection Agency, Research Triangle Park, NC 27711.

0018-9480/80/0700-0791$00.75 ©1980 IEEE

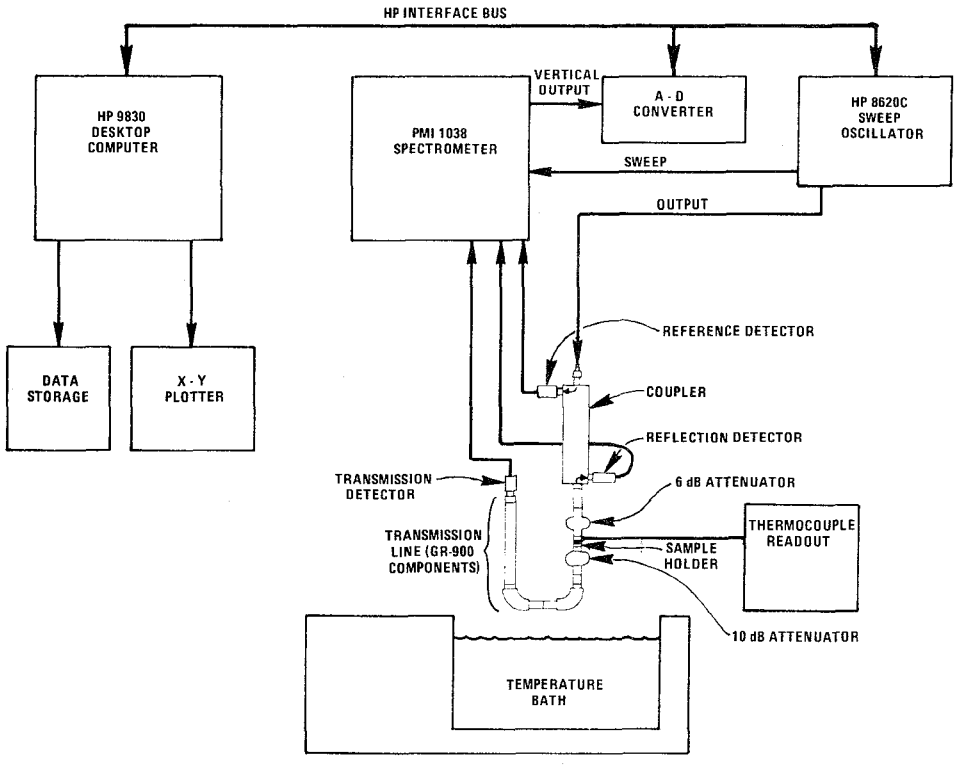

Fig. 1. Block diagram of the measurement system.

ise (at least for Debye spectra) but has not yet begun to produce routine data. Automated time-domain spectroscopy (TDS) methods also fulfill the basic requirements but have certain shortcomings. Existing TDS systems suffer from a high complexity of measurement technique (FFT, timing jitter, etc.) and have limited accuracy over some frequency ranges. In addition, current systems lose accuracy for sample conductivities greater than about 1.5 mho/m [6, p. 119]; they also have insufficient ability to study variations of permittivity with input power, as the field strength decay within the sample is a strong function of time (especially for the Thin Sample Method [7], [8]) and a power-dependent permittivity variation cannot be properly characterized.

This paper describes an automated swept-frequency absorption spectrometer which realizes significant improvement over existing methods. This instrumentation obtains all of the desired information (both broad-band and narrow-band absorption and permittivity data in both the frequency and power domains) through steady-state magnitude measurements. Measurement results reported here cover the range 0.1–2 GHz, which is the present range of the system; the frequency capability can be readily extended to other ranges, however. The system produces highly accurate absorption versus frequency plots and can produce differential plots wherein the difference between two absorption curves is plotted (in order to increase the possibility of finding small changes in the absorption characteristics of the sample(s)). The measurement procedure is very simple and rapid; once the sample holder is loaded the absorption data can be obtained in less than five minutes. The mathematics and programming involved are less complex than those of the TDS methods. The sample holder is designed for liquid samples but can be modified to accomodate solid or tissue samples. A very small volume of sample is required (approximately 0.15 ml), and the resulting constant steady-state field strength distribution throughout the sample makes for a good system to study power-dependency. The relaxation time τ of a molecule in solution is derived from the differential absorption plot (τ as used here is the actual molecular relaxation time as treated in the Debye theory of polar molecules in solution). The complex permittivity of the sample is derived using a computerized successive substitution technique. Accuracy of the permittivity results is comparable to that of many TDS methods, but unlike TDS systems, this new method can tolerate high sample conductivity to at least 6 mhos/m (equivalent to 0.7 molal NaCl in H_2O at 300 MHz).

II. Description of System Components

The system configuration is shown in Fig. 1. The principal component of the system is a Pacific Measurements, Inc. (PMI) swept frequency spectrometer. This unit is composed of a Model 1038 mainframe which contains two V12 Log Amp/Memory plugins and one H13 Horizontal/Memory/Log Amp plugin. With the associated PMI 12464 power detectors, this unit has a bandwidth from 1 MHz to 18 GHz, and is capable of acquiring and displaying continuous, swept-frequency magnitude curves (in

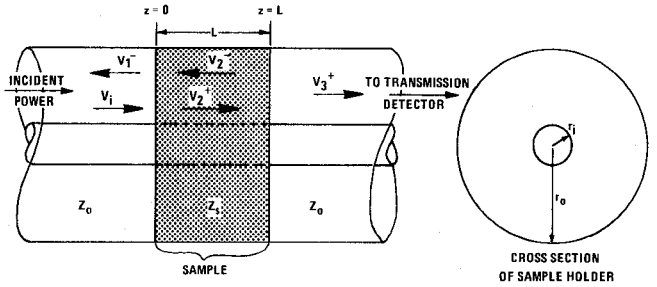

Fig. 2. Transmission line model used for calculations.

decibels) with better than 1-percent linearity (0.1 dB/10 dB). Each vertical plugin has a 1024-point×256-point memory which can store the various curves with an accuracy of ±0.08 dB or better; subtraction features enable an input curve to be subtracted from a calibration or reference curve stored in memory. The vertical plugin detectors are placed in the transmission line to measure both the reflected and the transmitted power from the sample. The third detector (reference) measures the input power to the line and provides for normalized measurements using a ratio (e.g., Transmitted/Incident, Reflected/Incident) feature of the PMI system. The signal source is a Hewlett-Packard 8620C Sweep Oscillator with an 86222B 0.01–2.4 GHz plugin currently installed. Control of the experiment and the acquisition and processing of the data are performed by an HP 9830 desktop computer interfaced to the instruments through an HP Interface Bus. A four channel ±1024 point A/D converter reads the voltage from the PMI's vertical deflection preamp and can provide the converted value to the computer. Four hundred points are typically sampled across the frequency band of interest; a step in the curve read procedure consists of the computer incrementing the oscillator frequency, then acquiring and storing a data point from the A/D converter, and then incrementing frequency again. The total scan time for one 400-point curve is approximately 45 s. Temperature control for the sample is obtained by covering the transmission line with a thin plastic bag and submerging it in a well-regulated (±0.1°C) temperature bath. Sample temperature is monitored by a thermocouple attached to the outer conductor of the sample holder.

III. Description of the Transmission Line

The transmission line consists of a set of General Radio GR-900 components fed from a Hewlett-Packard 778D dual directional coupler (measured directivity between 38 and 50 dB). The results reported in this paper cover the range 0.1–2 GHz, which is the nominal bandwidth of the coupler.

In the course of designing the sample holder, a mathematical model was developed to relate the permittivity and dimensions of the sample to the reflected and transmitted power, and hence to the absorbed power. Assuming TEM mode propagation, the following transmission line equations can be written for the three regions of the line shown in Fig. 2:

$$\left.\begin{aligned} V_1 &= V_i \exp(-jk_0 z) + V_1^- \exp(jk_0 z) \\ I_1 &= \frac{1}{Z_0}\left(V_i \exp(-jk_0 z) - V_1^- \exp(jk_0 z)\right) \end{aligned}\right\} z \leqslant 0 \quad \begin{matrix}(1a)\\(1b)\end{matrix}$$

$$\left.\begin{aligned} V_2 &= V_2^+ \exp(-jk_1 z) + V_2^- \exp(jk_1 z) \\ I_2 &= \frac{1}{Z_s}\left(V_2^+ \exp(-jk_1 z) - V_2^- \exp(jk_1 z)\right) \end{aligned}\right\} 0 \leqslant z \leqslant L \quad \begin{matrix}(1c)\\(1d)\end{matrix}$$

$$\left.\begin{aligned} V_3 &= V_3^+ \exp[-jk_0(z-L)] \\ I_3 &= \frac{1}{Z_0} V_3^+ \exp[-jk_0(z-L)] \end{aligned}\right\} z \geqslant L \quad \begin{matrix}(1e)\\(1f)\end{matrix}$$

($V_i = 1$ for normalized computations.)

$$\left.\begin{aligned} &1)\quad V_1 = V_2 \text{ at } z=0 \\ &2)\quad I_1 = I_2 \text{ at } z=0 \\ &3)\quad V_2 = V_3 \text{ at } z=L \\ &4)\quad I_2 = I_3 \text{ at } z=L \end{aligned}\right\} \text{Boundary Conditions} \quad \begin{matrix}(2a)\\(2b)\\(2c)\\(2d)\end{matrix}$$

where

$$jk = \alpha + j\beta \tag{3}$$

$$\hat{\epsilon} = \epsilon' - j\epsilon'' \tag{4}$$

(ϵ'' used here is the dipolar loss only)

$$\alpha = \omega\left\{\left(\frac{\mu_0\epsilon'}{2}\right)\left[\left(1+\left(\frac{\epsilon''}{\epsilon'}\right)^2\right)^{1/2} - 1\right]\right\}^{1/2} \tag{5}$$

$$\beta = \omega\left\{\left(\frac{\mu_0\epsilon'}{2}\right)\left[\left(1+\left(\frac{\epsilon''}{\epsilon'}\right)^2\right)^{1/2} + 1\right]\right\}^{1/2} \tag{6}$$

$$Z_s = \left(\frac{R+j\omega L}{G+j\omega C}\right)^{1/2} \tag{7}$$

$$Z_0 = 50\ \Omega \tag{8}$$

$$R = \frac{R_s}{2\pi}\left(\frac{1}{r_0}+\frac{1}{r_i}\right), \qquad R_s \cong 3.1\times 10^{-7}(f)^{1/2} \text{ for gold} \tag{9}$$

$$L = \frac{\mu_0}{2\pi}\ln\left(\frac{r_0}{r_i}\right) \tag{10}$$

$$C = \frac{2\pi\epsilon'}{\ln(r_0/r_i)} \tag{11}$$

$$G = \frac{2\pi\omega\epsilon''}{\ln(r_0/r_i)}. \tag{12}$$

A computer program was written which uses these equations to calculate the magnitudes of the transmitted, reflected, and absorbed power when given the length and the complex permittivity of the sample. These calculations were corrected for wall loss and ionic conductivity using a method taken from Grant [6, pp. 91–93].

Studies based on this computer program have shown that the highest sensitivity to permittivity variations occurs for very short samples ($L \cong 1.0$ mm). Additionally, if the length L is of the order of one-quarter wavelength or

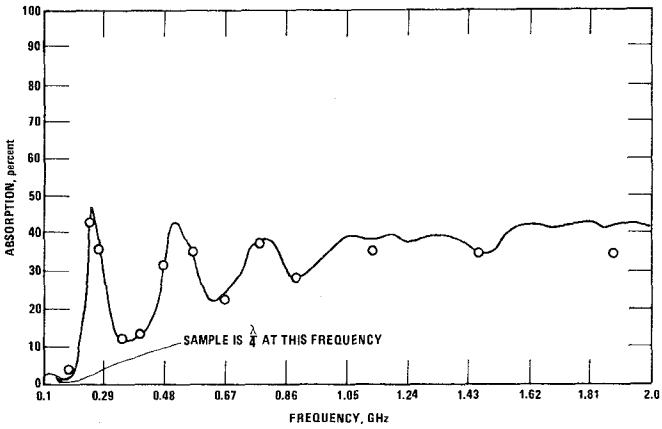

Fig. 3. Measured response of a 6-cm length of 0.25-M triglycine solution in H_2O. Length-dependent resonance effects are clearly evident. The circles represent the predicted absorption based on permittivity data.

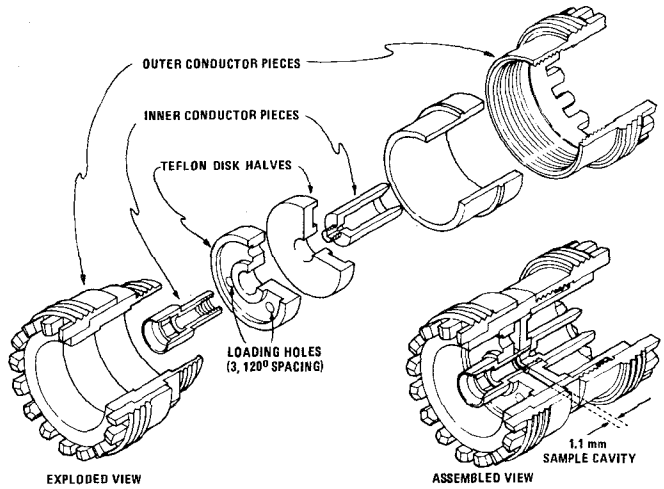

Fig. 4. Detail of the sample holder showing the modifications made to the GR 900-L3 3-cm air line.

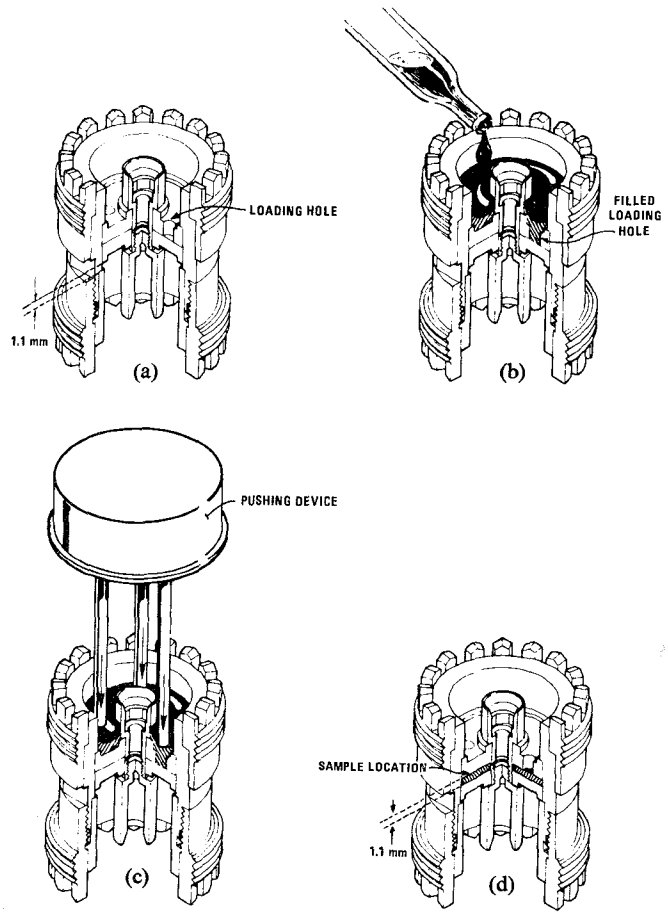

Fig. 5. Sample holder loading procedure. (a) Both Teflon pieces are pressed together and seated against upper stop. (b) Sample liquid is loaded; all air bubbles are removed from loading holes. (c) Pushing device forces bottom bead against lower stop; suction draws liquid into chamber. (d) Excess liquid is drawn off; loading holes are cleared.

larger in the band of interest, resonant peaking occurs due to the $(2n+1)\lambda/4$ transformer effects of the sample. Fig. 3 depicts the measured results of this behavior for a 6-cm column of 0.25-M aqueous triglycine solution in air line. The circles in the figure represent predicted values of absorption based on permittivity data from Lawinski *et al.* [9].

A sample holder which uses a sample length L of 1.1 mm was designed and constructed; for most samples of interest this places the $\lambda/4$ dip at approximately 8 GHz. A GR 900-L3 3-cm air line was modified as shown in Fig. 4. A Teflon disk was cut latitudinally in half and the resulting two new faces were shaved to a smooth finish with a microtome. The sample occupies the resulting cavity, the thickness of the removed material being 1.1 mm. Three 0.073-in diameter holes were drilled in the top Teflon piece to facilitate loading. To determine the effect of the holes on the characteristic impedance, an uncut disk was similarly drilled to a depth of approximately 2.5 mm and then inserted into an air line. Return loss measurements indicated that the characteristic impedance had changed by less than 1 percent, i.e. the impedance of the air line in the region of the drilled piece is between 50 and 50.5 Ω. This impedance alteration was judged to be negligible for the current set of experiments and was not incorporated into the data analyses programs.

A multiple-step procedure is required to load the sample holder (Fig. 5). Both halves of the Teflon disk are mounted on the center conductor, the whole arrangement then being pressed into the outer conductor (a tight force fit) and seated firmly against the upper stop. Note that both halves are pressed firmly together to squeeze all air from between them, and that the lower half is positioned 1.1 mm above the lower stop. Sample liquid is then introduced into the space above the Teflon and is forced into the three holes; a small instrument such as a syringe is used to clear air bubbles from the holes. A pushing device having three 1/16-in metal, glass, or plastic prongs is used to force the bottom Teflon piece against the lower stop. These prongs fit in each of the three holes in the top Teflon piece and have a slightly smaller diameter than the holes; thus when the bottom bead is forced downward, the suction draws the liquid along the prongs and into the

cavity. Loading is completed when the excess liquid is removed from the space above the Teflon and from the three holes. This has proven to be an excellent loading procedure—the sample holder has been X-rayed after several loadings and no air bubbles have been detected. Bubbles can form, however, within the sample during the course of an experiment which employs elevated sample temperatures, as gases are forced out of solution by the decreased gaseous solubility. This problem is eliminated by using fresh solutions made from solvents which have been recently deionized or otherwise degassed, or have been stored at elevated temperatures.

A transmission line error analysis was performed using techniques in [10]. In particular, it can be shown that the expression for maximum expected error in a reflection measurement is

$$E_{\max} \cong A + \rho_s \rho_u^2 \tag{13}$$

where A is the coupler directivity, ρ_s is the effective source match as seen from the sample, and ρ_u is the magnitude of the reflection coefficient of the sample. Similarly, the uncertainty in a transmission measurement can be shown to have the following form:

$$U_{\max} \cong \frac{(1 \pm \rho_s \rho_D)}{(1 \pm \rho_s \rho_u)(1 \pm \rho_u \rho_D) \pm (\rho_s \tau_u^2 \rho_D)} \tag{14}$$

where ρ_s is the effective source match seen from the sample, ρ_D is the magnitude of the reflection coefficient seen by the sample looking toward the transmission detector, ρ_u is the magnitude of the reflection coefficient of the sample, and τ_u is the magnitude of the sample transmission coefficient. A significant reduction in measurement errors is realized if the ρ_s and ρ_D terms are reduced in value. It has been determined that ρ_s over 0.1–2 GHz for the line without the attenuators installed is $\leqslant 0.029$ (corresponding to a VSWR of 1.05) and that ρ_D is $\leqslant 0.056$ (corresponding to a VSWR of 1.12). For a transmission measurement, the 6-dB and 10-dB General Radio attenuators in the line accomplish such an error reduction, as their input VSWR is < 1.02 below 2 GHz and the original ρ_s and ρ_D values are considerably reduced by the attenuation. Such added attenuation in the line does degrade the signal-to-noise ratio, but the effects are negligible for oscillator outputs above -7 dBm. The minimum vector errors for a reflection measurement are obtained with the 6 dB attenuator removed and replaced with a straight section of air line. The magnitude of ρ_s is of course reduced with the attenuator in place, but since the reflected power is reduced by 12 dB the directivity becomes the dominant error term. Thus for maximum accuracy two measurement runs must be made, one for the transmission measurement(s) and one for the reflection measurement(s).

The noise floor of the PMI system has been observed to rise as the detectors are cooled below room temperature. This effect appears to originate in the temperature compensation circuitry built into each detector. To minimize this condition a 30-cm air line is used to support the transmission detector above the water level of the temperature bath. Both the reflection and the transmission detectors are still somewhat coupled to the bath by the thermal conduction of the transmission line. The slight temperature-induced offset shifts that occur in the measured curves are easily characterized and compensated for by the computer.

IV. Operating Procedures

The transmission and reflection curve acquisition is a straightforward procedure. For the transmission measurement, a calibration curve is first obtained without the sample in place to account for coupling factor anomalies and miscellaneous line losses. This curve is stored in the PMI memory and is internally subtracted from the line-with-sample curve to obtain the final normalized and corrected transmission curve. Calibration for the reflection measurement is a bit more involved. The Short/Open Method is used [10] where a short circuit is placed in the line at the sample position and the reflection curve is stored in the computer, then an open circuit is placed in the sample position and its respective curve is stored in the computer. A short program routine averages these curves to produce a calibration curve which essentially represents corrections for tracking errors and primary line residual losses. This curve is then subtracted by the computer from the line-with-sample reflection curve before further computations.

Various other correction and calibration features are also required. The Reference detector system has zero sensitivity below signal levels of -30 dbm, therefore the oscillator output must be held above -10 dbm (for a 20-dB coupling factor). If lower power levels are desired, one may use either of the vertical plugin systems for the reference. The vertical drive circuitry in the PMI has a SMOOTHING (low-pass filter) feature which can be used at very low sweep rates ($\geqslant 5$ s/sweep) to effectively improve the signal-to-noise ratio for low-power measurements. Before the General Radio attenuators were installed, it was noted that for highly reflective samples and at high power outputs the oscillator produced a significant amount of harmonics and AM/FM noise. A 10-dB pad on the output of the oscillator has thus far remedied this condition. Without the 10-dB pad, an artifact can be produced in an investigation of power-dependent properties, where one simply varies the oscillator power and watches for variations in the displayed curves. Using procedures described in the PMI User's Manuals, one can determine the calibration errors of the instrument to a good accuracy; the respective offset and linearization corrections can be incorporated into the computer routines.

A summary of instrument error due to all sources is given in Table I. In order to quantify the random error of the spectrometer measurements, four separate but identical runs were made with deionized water at 25°C. The standard deviation of the runs was computed at each of the 400 points of the absorption curve; the average of

TABLE I
CALCULATED MAXIMUM INSTRUMENT ERRORS AT TWO COMMON FREQUENCIES FOR A TYPICAL AQUEOUS SAMPLE

Source	@ 0.47 GHz		@ 1.46 GHz	
	Transmission	Reflection	Transmission	Reflection
PMI Memory (±0.0155 dB)	0.36% of meas. value	NA	0.36% of meas. value	NA
PMI Linearity (0.01dB/dB)	0.3% o.m.v.	1.9% o.m.v.	1.1% o.m.v	0.83% o.m.v.
Line mismatch errors	0.3% o.m.v.	2.89% o.m.v.	1.1% o.m.v.	4.7% o.m.v.
A-D Converter (Transm.: ±.005dB) (Refl.: ±.025dB)	0.115% o.m.v.	0.57% o.m.v.	0.11% o.m.v.	0.57% o.m.v.

these was then taken, producing a negligible average standard deviation of 0.27 percent. The predominant random error mechanism probably arises from uncertainties in the offset calibration procedures for the PMI which are followed before each experiment. Thus, one may conclude that the sample holder configuration and the loading procedure produce consistent results, and that in general the repeatability of these measurements is excellent.

V. Derivation of Complex Permittivity

The derivation of the complex permittivity from the normalized percentages of transmitted, reflected, and absorbed power uses a rather straightforward technique. Equation (1) can be substituted into the boundary conditions of (2) to produce four equations in the variables V_1^-, V_2^+, V_2^-, V_3^+, ϵ', ϵ'', and ω. Manipulation results in the elimination of V_2^+ and V_2^- and a reduction of these equations to two expressions, one for V_1^- and one for V_3^+. The magnitudes of both sides of these expressions may be taken and then squared to produce two equations in two unknowns, ϵ' and ϵ'', where $|V_1^-|^2$ and $|V_3^+|^2$ become the measured values of reflected and transmitted power, respectively (recall that V_t is unity). These equations provide a solution for ϵ' and ϵ'' for all physically meaningful values of complex permittivity. This fact has been confirmed at 0.47 GHz by an examination of computer-generated tables of transmitted and reflected power, where ϵ' and ϵ'' were used as parameters which varied from 1 to 1000 for ϵ_r' and from 0 to 1000 for ϵ_r''. In practice, a unique solution may be prevented by ambiguities concerning the signs of terms which contain square roots and fourth roots. Even where unique solutions are realized, the various instrumentation errors can produce large deviations in the permittivity results.

A successive-substitution technique which minimizes these problems has therefore been implemented. ϵ' and ϵ'' are substituted as incremented parameters into the equations for V_1^- and V_3^+ and the resulting calculated values of transmission, reflection, and absorption are compared with the measured values to determine the correct ϵ' and ϵ''. To initiate the process, the operator feeds in a good first guess of the permittivity values (based on a generated table of permittivity versus transmitted and reflected power) at some particular midband frequency. The program then searches about these values, decides on the most correct ones, stores them, and then increments frequency and uses the newly stored values as the new first guess. The measured transmitted, reflected, and absorbed powers are independently used to select three separate values of ϵ' or ϵ''. There will generally be slight disagreement; the final value of ϵ' or ϵ'' is determined by a simple average of the three. Some improvement in accuracy may be noted by using a weighted average, where one measurement might be more accurate than another. Aside from measurement uncertainties in the transmitted and reflected power, the accuracy of this procedure is governed only by the size of the search window about the first guess and by the size of the increments through which the trial ϵ' and ϵ'' are stepped. This technique always yields a unique solution; additionally, the effects of instrumentation errors and random noise are reduced by the independent selection and averaging procedure.

VI. Discussion of Performance

To characterize the performance of this system, measurements were taken over a series of temperatures with samples of both deionized water and 0.25-M triglycine solution in deionized water. The triglycine for these experiments was obtained from Sigma Chemical Company, St. Louis, MO. Temperatures of 5°, 12.5°, 20°, 30°, and 40°C were chosen to coincide with the data of Lawinski *et al.* [9] to facilitate comparison of results. The conductivity of these solutions at 25°C as measured at 1 kHz with a Leeds and Northrup Model 4959 bridge was 1.97×10^{-5} mhos/m for the deionized water and 2.08×10^{-3} mhos/m for the triglycine solution. Plots of the measured transmitted and reflected power over the range 0.1–2 GHz for triglycine at 20°C are given in Figs. 6 and 7, respectively. These curves are representative of the overall results. The circles represent calculated values derived from the permittivity data of Lawinski. Good agreement is noted for the transmission curve except that a negative offset, with respect to the calculated values, occurs which exhibits significance above roughly 900

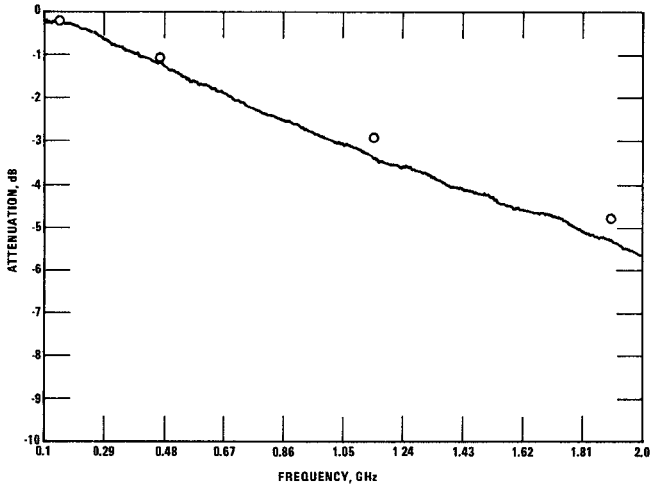

Fig. 6. Transmission loss measurement for 0.25-M triglycine solution at 20°C. The circles represent calculated values.

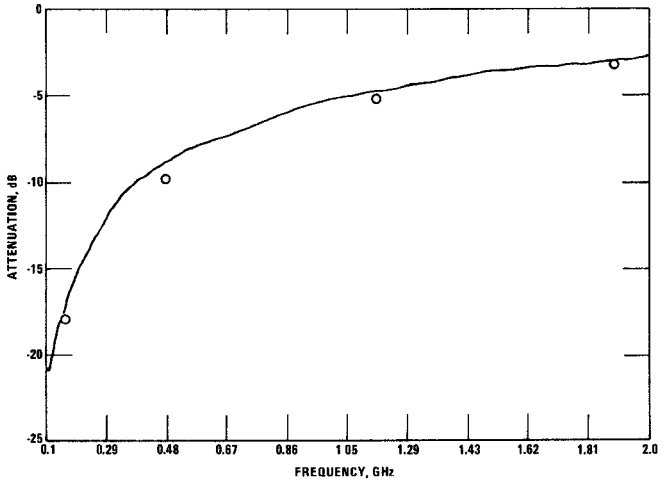

Fig. 7. Return loss measurement for 0.25-M triglycine solution at 20°C. The circles represent calculated values.

MHz. The reflection curve shows similar agreement, but displays an approximately constant positive offset with respect to the calculated values.

The small deviations from perfect agreement are due to a variety of possible factors. The disagreement above 900 MHz for the transmission curve and the positive offset of the reflection curve are probably due to sample holder characteristics. At first glance the reflection curve offset appears to arise from an ignorance of some fairly constant correction factor; however, reflection measurements on deionized water display essentially perfect agreement which argues that this offset is a function of the electrical properties ($\hat{\epsilon}$) of the sample. Calculations based on the dimensions of the sample holder and the sample permittivity reveal that higher order modes can propagate within the sample at frequencies above roughly 900 MHz. Such mode mixing will violate the TEM condition on (1) and will thus lead to disagreement. Work by Green [11] indicates that field distortions due to the step discontinuities in the conductors at the Teflon disk-to-air transitions may be significant at the sample interfaces, and would thus produce such a non-TEM field structure. Other factors which might account for such effects are the possible slight nonparallelism of the flat faces of the sample and also the fact that small liquid columns can exist in each of the three loading holes. These factors would not only provide mode excitation but would produce uncertainties in the apparent electrical length L of the sample. Line mismatch errors are noted in these curves to be relatively smooth, periodic undulations (most apparent in the transmission curve above 1 GHz). Further sources of disagreement are of course small contributions from other instrument and random error mechanisms, and also possible anomalies in Lawinski's data.

The power absorption curves of triglycine versus frequency over the series of temperatures are given in Fig. 8. The circles again represent predictions derived from the data of Lawinski *et al.* [9]. Agreement is generally good, and the results demonstrate consistency over temperature. The fact that the measured absorption is occasionally higher than the predicted above roughly 300 MHz is due to the aforementioned transmission and reflection curve offsets. The slight disagreement below 200 MHz is due to a small calibration uncertainty in the transmission curves. Periodic undulations above 700 MHz are manifestations of the line mismatch errors.

Fig. 9 shows differential plots over the temperature series, obtained by subtracting the absorption curves of deionized water from those of the 0.25-M triglycine solution given in Fig. 8. These plots represent the portion of the total absorption which is due solely to the presence of the relaxing triglycine molecule in solution. Errors such as the line mismatch errors are contained in both absorption curves and are essentially eliminated by the subtraction. The differential plot affords a convenient method of determining the relaxation time τ of a molecule; likewise any subsidiary absorption region due, for example, to side chain or bound water resonances can be identified and characterized.

The derivation of τ is accomplished through a simple procedure. The peaks of the differential plot do not necessarily correspond to the relaxation frequencies or relaxation times of the specific molecular components of a solution. However, it is well known that the frequency of maximum local enhanced absorption lies at the point where ϵ'' exhibits a local maximum and where ϵ' displays an inflection point. The first derivative of the Debye expression for ϵ'' with respect to ω can be used together with a knowledge of these frequencies to determine the various relaxation times τ_n of solution components. If measurement system bandwidth is sufficient for all of these frequencies to be identified, then the τ_n may be found by solving sets of simultaneous equations. These equations are obtained by setting the expression for the ϵ'' derivative equal to zero at each of the peak frequencies ω_k. It should be noted that the relaxation time for a solvent may change appreciably with the addition of

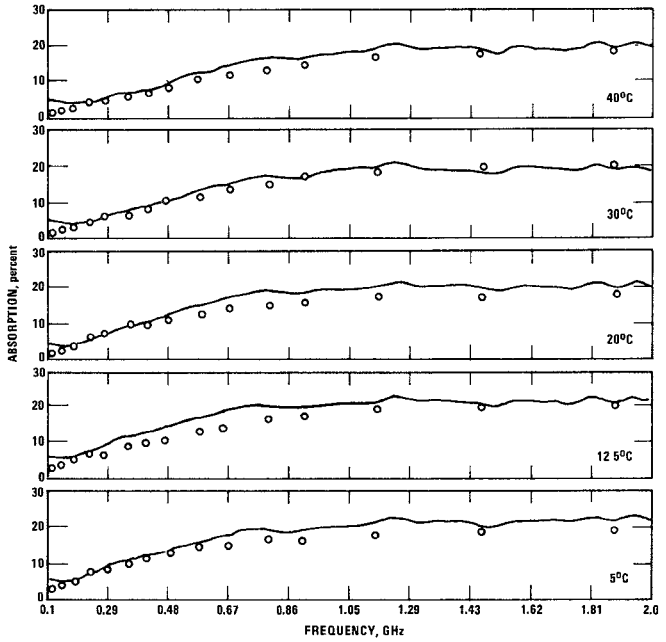

Fig. 8. Absorption versus frequency over a series of temperatures for 0.25-M triglycine solution. The circles represent predicted values based on the permittivity data from Lawinski *et al.* [9].

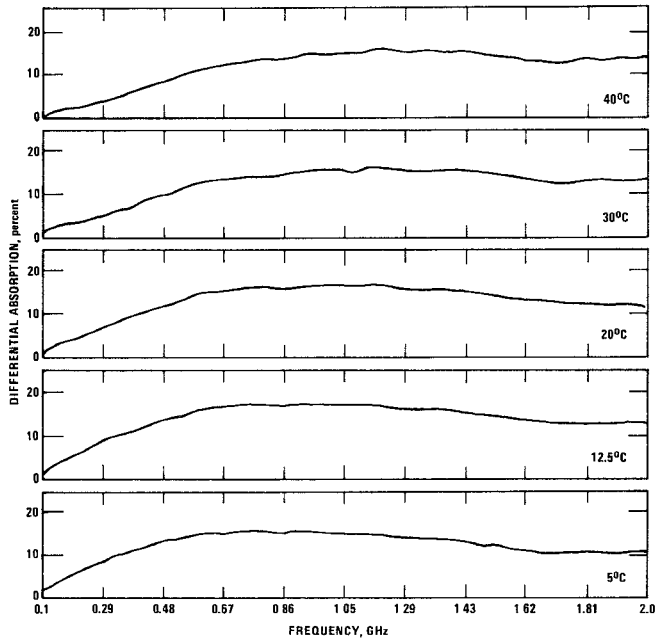

Fig. 9. Differential absorption for triglycine solution over temperature. The upward shift of relaxation frequency with temperature is readily apparent.

solute(s). If this is the case, then a peak will appear on the differential plot which corresponds approximately to this new relaxation time (the exact position of the peak is given by the various Debye expressions). If the solvent's relaxation time does not change significantly, the differential plot will display no real peak in this region; therefore, one must use the frequency of the absorption peak which occurs on the solvent's absorption plot.

A similar approach, has been undertaken using the differential plots of Fig. 9. Specifically, for a two-component solution (triglycine in H_2O) the Debye equation is

$$\epsilon' - j\epsilon'' = \epsilon_\infty + \frac{\Delta_1}{1+j\omega\tau_1} + \frac{\Delta_2}{1+j\omega\tau_2} \tag{15}$$

where

Δ_1 $= \epsilon_s - \epsilon_m$;
ϵ_s low frequency static value of ϵ';
ϵ_m value of ϵ' at frequencies between the solute and the solvent dispersions;
Δ_2 $= \epsilon_m - \epsilon_\infty$;
ϵ_∞ value of ϵ' at frequencies far above the dispersions;
τ_1, τ_2 the relaxation times of the solute and the solvent, respectively, in the particular solution.

Taking the imaginary part of expression (15) and differentiating with respect to ω gives

$$\frac{d\epsilon''}{d\omega} = \frac{\Delta_1\tau_1}{1+\omega^2\tau_1^2} + \frac{\Delta_2\tau_2}{1+\omega^2\tau_2^2} - \omega^2\left[\frac{2\Delta_1\tau_1^3}{(1+\omega^2\tau_1^2)^2} + \frac{2\Delta_2\tau_2^3}{(1+\omega^2\tau_2^2)^2}\right]. \tag{16}$$

This equation can be set equal to zero and solved for τ_1 at some radian frequency ω_k where ϵ'' exhibits a local peak. The parameters which must be known for this operation are τ_2, ω_k, Δ_1, and Δ_2. The relaxation peak at roughly 20 GHz, which is primarily due to the water molecules, cannot be obtained with the present measurement system bandwidth (0.1–2 GHz). Thus, τ_2 must be found by other means and can often be taken directly or estimated from literature values such as those in [9]. ω_k is easily obtained from the differential plot, and Δ_1 and Δ_2 may be estimated using a method outlined in [9]. This method requires the knowledge of ϵ_s and ϵ_∞ of the solution and possibly ϵ_s of the pure solvent. ϵ_∞ may either be estimated or measured, ϵ_s of the solution may be estimated from the permittivity derivation or accurately measured at a single low frequency using a bridge technique, and ϵ_s of the solvent may be found in the literature. Thus, there is relatively little difficulty in obtaining the information necessary to derive τ_1. Table II provides a comparison of relaxation times computed by this method to those obtained by

TABLE II
COMPARISON OF MEASURED RELAXATION TIMES WITH LITERATURE VALUES

Temperature (°C)	Relaxation time τ_1, (in psec) Measured	From Lawinski et al. [9] (value ± 95% confidence interval)	% Discrepancy
40	165	170 ± 8	2.9
30	177	197 ± 8	10 1
20	228	258 ± 12	11.6
12.5	294	324 ± 19	9 2
5	370	415 ± 28	10.8

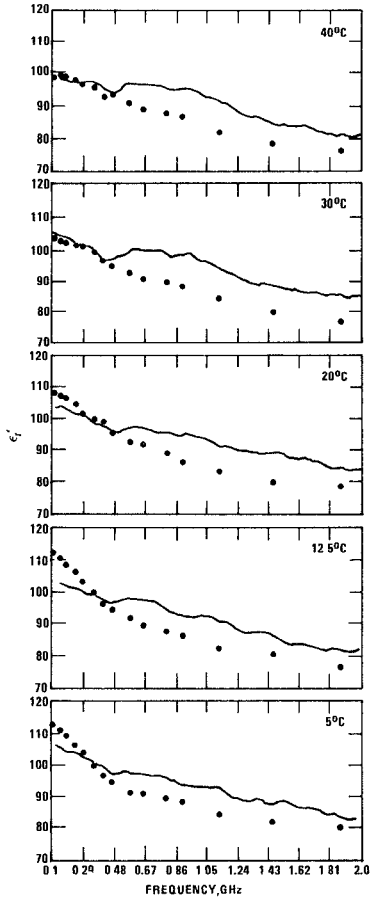

Fig. 10. The real part of complex relative permittivity as derived from the magnitude measurements on triglycine solution. The permittivity data of Lawinski *et al.* [9] are plotted as points for comparison.

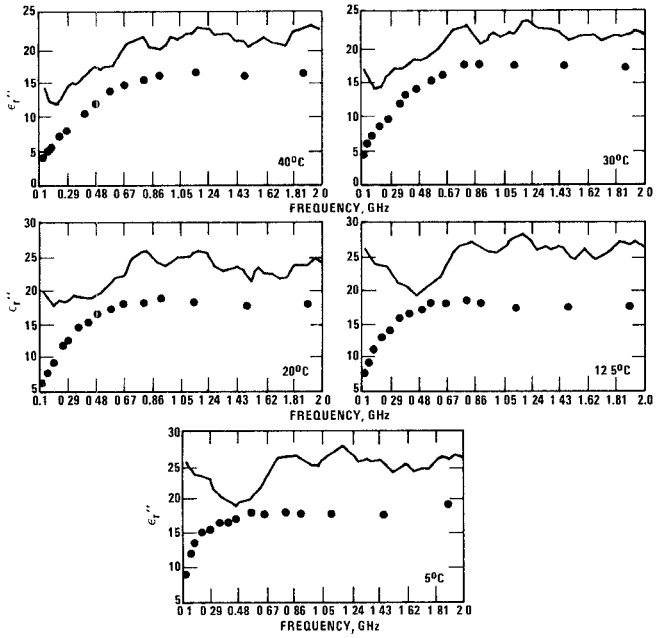

Fig. 11. The imaginary part of complex relative permittivity as derived from the magnitude measurements on triglycine solution. Lawinski's data points are plotted for comparison.

Lawinski *et al.* [9] using a curve-fitting procedure. Values for Δ_1, Δ_2, and τ_2 used in these computations were taken from [9].

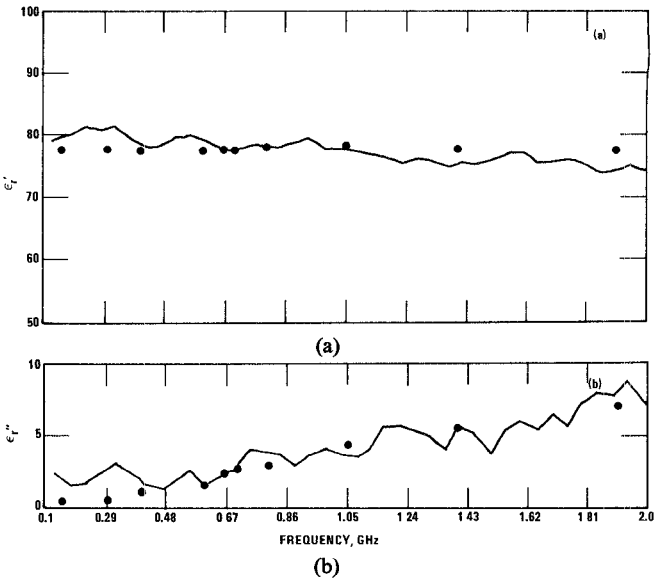

Fig. 12. Real part (a) and imaginary part (b) of the complex relative permittivity of deionized water at 25°C as calculated from magnitude measurements. The points represent values from Schwan *et al.* [12].

Figs. 10 and 11 show plots of relative ϵ' and ϵ'' (where $\hat{\epsilon}_r = \epsilon_r' - j\epsilon_r''$), respectively, as derived from the magnitude measurements of the 0.25-M triglycine solution. The computer routine which derived this information was programmed to examine the range covering ± 2 permittivity points from the initial guess, and to increment ϵ_r' trial values by 0.5 and ϵ_r'' trial values by 0.2. The dots again represent values taken from Lawinski *et al.* [9]. Good agreement is noted for ϵ_r' in Fig. 10—the error is 11 percent or less over the entire range. The discrepancies become larger above 0.47 GHz as a result of the increasing dominance of the transmission and reflection curve offset errors. Discrepancies in ϵ_r'' in Fig. 11 for the range above 0.29 GHz generally vary from 20 to 30 percent, and are again due to the measured curve offset errors. The increasing disagreement in ϵ_r'' below 0.29 GHz (particularly evident for the lower temperatures) is primarily a result of the transmission curve calibration uncertainties in this region.

Fig. 12 gives plots of both ϵ_r' and ϵ_r'' for deionized water at 25°C. The dots represent the data of Schwan *et al.* [12]. Excellent agreement is noted, especially for ϵ_r' where the discrepancy is 4 percent or less. The accuracy of these measurements is seemingly better than that for the triglycine measurements, owing to the fact that the transmission and reflection curve offset errors are not as great. This is in accord with the earlier observation that the offsets have some dependence on the electrical properties of the sample.

To improve the accuracy of permittivity results, several more sophisticated sample holder analyses have been undertaken in order to better understand the transmission and reflection curve offset errors. The most successful to date involves a program which adjusts the variable for the length L of the sample so as to force the calculated ϵ_r' and ϵ_r'' values to match Lawinski's data at a single frequency of 0.9 GHz. This adjusted value of L is then used for all

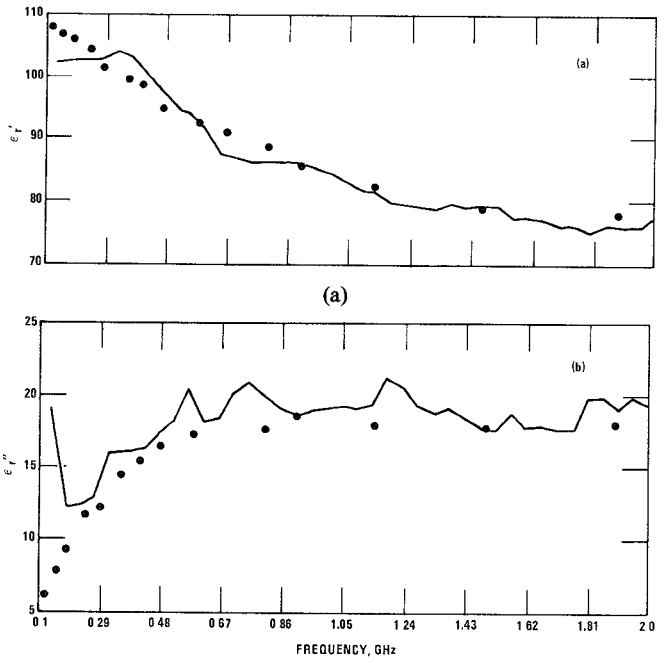

Fig. 13. Real part (a) and imaginary part (b) of the complex relative permittivity of the triglycine solution at 20°C as derived using a program which compensates for possible field distortions at the sample faces. Lawinski's data points are plotted for comparison.

subsequent permittivity calculations across the entire frequency range. Trial runs for all five temperatures reveal that a lengthening in L of 10 percent or less is required to produce excellent permittivity accuracy. Fig. 13 gives a typical example of results for ϵ_r' and ϵ_r'' at 20°C for the 0.25-M triglycine solution. The disagreement in ϵ_r' varies from 0 percent to no more than 4 percent, and the disagreement for ϵ_r'' varies from 0 percent to about 20 percent (below 0.15 GHz the transmission curve calibration uncertainty produces larger errors). This is strong evidence to support the view that field distortions do occur at the sample faces and that they act to increase the apparent electrical length of the sample. The above analysis is an empirical one, however, and contributions from other sources, such as higher order mode propagation, cannot yet be discounted. Investigation of these questions continues with the hope of developing a more refined model of the field structure in the sample holder region of the transmission line.

Computer studies based on (1) and (2) have shown that this measurement system is relatively immune to sensitivity loss when using samples of high conductivity. An accuracy in permittivity of 10 percent or better is predicted for the measurement of a sample of conductivity equal to 6 mhos/meter (equivalent to 0.7-M NaCl solution in H_2O, where $\epsilon_r' \cong 66$ and $\epsilon_r'' \cong 370$ at 300 MHz as estimated from von Hippel [13]).

VII. Conclusion

A new technique for dielectric measurements has been presented. Primary advantages and features of the measurement system include the following.

1) The system produces highly accurate, continuous plots of absorption and differential absorption versus frequency.

2) Continuous plots of complex permittivity can be produced. The measurement accuracy of permittivity and relaxation time τ, while not quite as good as fixed-frequency methods, is equal to or better than that of many TDS systems (see for example Clark *et al.* [8], where roughly 15-percent accuracy was obtained for τ for several solutions).

3) Measurement procedures are simple and rapid, which enables among other things the study of time-varying processes.

4) Only steady-state magnitude measurements are involved; therefore much of the equipment is relatively inexpensive when compared to a network analyzer system, and the experimental techniques and analysis required are less complex than those of TDS methods.

5) System sensitivity is approximately constant for values of sample conductivity up to at least 6 mhos/m.

6) Very small volumes of sample (0.15 ml) are required, which is an advantage if the sample is expensive or scarce, and

7) Power density dependencies of various sample properties may be easily investigated by manually varying the input power to the transmission line, as field strength remains roughly constant throughout the length of such a short sample.

Capabilities and limitations of the current system are defined as follows.

1) The maximum incremental frequency resolution limit is 100 kHz.

2) The bandwidth, presently 0.1–2 GHz, depends heavily on the availability of quality directional couplers and signal sources. With a suitable source and high-directivity coupler, the General Radio GR-900 air line configuration should provide useful data up to its maximum usable frequency of 8 GHz. Measurements above this region should be possible using a sample holder system made of smaller diameter coaxial lines or waveguide. Resonant length effects will appear above 8 GHz for a sample length of roughly 1 mm, but these should not affect the differential plots or the permittivity results. There is also an increasing loss of sensitivity to sample permittivity as the wavelength becomes smaller with respect to sample length, but studies indicate that the data will be usable up to at least the 10–15-GHz range.

3) Small-magnitude differential absorption and power-specific responses can be resolved to within approximately ± 0.27 percent, which is one standard deviation of the measurements due to random error.

4) The present range of usable incident power to the sample covers roughly -40 dBm to some arbitrary high value which depends on the signal source. The lower limit could be improved through the use of more sophisticated detection circuitry.

5) The present sample holder only accomodates liquid samples. Mechanical modifications could easily be made to permit the loading of solid or tissue samples.

Additional work is underway to improve the accuracy and extend the frequency range of the current measurement system. More sophisticated sample holder modeling techniques are being investigated in order to enhance the accuracy of the permittivity measurements. Another point being examined is the possibility of deriving $\hat{\epsilon}$ of a solution by using the differential plot and a knowledge of $\hat{\epsilon}$ of the solvent, since this procedure seems insensitive to many of the error mechanisms. The system is also being reconfigured to provide an automated power-sweep capability to enable fixed-frequency power domain measurements. Further experimental work is directed toward identifying and quantifying any (narrow-band?) frequency and/or power-specific responses in complex chemical and biological systems. Ultimately, it is hoped that the information obtained in this manner will be useful not only in fundamental studies of dielectric properties but also in the design of biological experiments which involve responses that may have frequency or field strength dependencies.

ACKNOWLEDGMENT

Thanks are due R. Baudendistel and W. Parrot for assistance in the construction of several components. The help of Barbara Sinha in preparing the sample solutions is appreciated. The authors also wish to thank Dr. W. T. Joines for valuable discussions.

REFERENCES

[1] S. M. Bawin, L. K. Kaczmarek, and W. R. Adey, "Effects of mediated VHF fields on the central nervous system," in *Biologic Effects of Nonionizing Radiation, Ann. N.Y. Acad. Sci.*, vol. 247, pp. 74–81, Feb. 1975.

[2] C. F. Blackman, J. A. Elder, C. M. Weil, S. G. Benane, D. C. Eichinger, and D. E. House, "Induction of calcium-ion efflux from brain tissue by radio-frequency radiation: Effects of modulation frequency and field strength," Special Supplement, Biological Effects of Electromagnetic Waves, *Radio Sci.*, 1979.

[3] C. E. Tinney, J. L. Lords, and C. H. Durney, "Rate effects in isolated turtle hearts induced by microwave irradiation," *IEEE Trans. Microwave Theory Tech.*, vol. MTT-24, pp. 18–24, Jan. 1976.

[4] S. M. Bawin, A. Sheppard, and W. R. Adey, "Possible mechanisms of weak electromagnetic field coupling in brain tissue," *Bioelectrochem. Bioenergetics*, vol. 5, pp. 67–76, 1978.

[5] M. L. Swicord, "Broadband measurements of dielectric properties," in *Proc. Symp. Biological Effects and Measurement of Radio Frequency/Microwaves*, HEW publication (FDA) 77-8026, Rockville, MD, July 1977.

[6] E. H. Grant, R. J. Sheppard, and G. P. South, *Dielectric Behaviour of Biological Molecules in Solution*. Oxford, England: Clarendon Press, 1978.

[7] H. Fellner-Feldegg, "A thin-sample method for the measurement of permeability, permittivity, and conductivity in the frequency and time domain," *J. Phys. Chem.*, vol. 76, no. 15, pp. 2116–2123, 1972.

[8] A. H. Clark, P. A. Quickenden, and A. Suggett, "Multiple reflection time domain spectroscopy," *J. Chem. Soc. Faraday Trans. II*, vol. 70, pp. 1847–1861, 1974.

[9] C. P. Lawinski, J. C. W. Shepherd, and E. H. Grant, "Measurement of permittivity of solution of small biological molecules at radiowave and microwave frequencies," *J. Microwave Power*, vol. 10, pp. 147–162, July 1975.

[10] Hewlett Packard Co. Application Note 183, "High frequency swept measurements," Nov. 1977

[11] H. E. Green, "The numerical solution of some important transmission-line problems," *IEEE Trans. Microwave Theory Tech.*, vol. MTT-13, pp. 676–692, 1965.

[12] H. P. Schwan, R. J. Sheppard, and E. H. Grant, "Complex permittivity of water at 25°C," *J. Chem. Phys.*, vol. 64, pp. 2257–2258, 1976.

[13] A. R. von Hippel, Ed., *Dielectric Materials and Applications*. Cambridge, MA: MIT Press, 1954, p. 361.

Irradiation of Prolate Spheroidal Models of Humans in the Near Field of a Short Electric Dipole

MAGDY F. ISKANDER, MEMBER, IEEE, PETER W. BARBER, MEMBER, IEEE, CARL H. DURNEY, MEMBER, IEEE, AND HABIB MASSOUDI, MEMBER, IEEE

***Abstract*—Analysis of the near-field irradiation of prolate spheroidal models of humans and animals by a short electrical dipole is described. The method of solution involves an integral equation formulation of the problem in terms of the transverse dyadic Green's function and expanding the fields irradiated by a short dipole in terms of the vector spherical harmonics. The extended boundary condition method (EBCM) is employed to solve the integral equations. The power distribution and the average specific absorption rate (SAR) are calculated and plotted as a function of the separation distance. It is shown that for a dipole placed along the major axis of the spheroidal (k-polarization [1]), and for a very short separation distance, $d = 0.15\ \lambda$, the relative power values at both ends of the spheroid are about 40 compared with the ratio of 15 in the planewave exposure case. Furthermore, the calculated average SAR values**

Manuscript received September 14, 1979; revised January 24, 1980.

The authors are with the Department of Electrical Engineering, University of Utah, Salt Lake City, UT 84112.

0018-9480/80/0700-0801$00.75 ©1980 IEEE